Fall 12-9-2022

WEARABLE SENSORS FOR PLANTS

Nafize Ishtiaque Hossain

WEARABLE SENSORS FOR PLANTS

by

NAFIZE ISHTIAQUE HOSSAIN

A thesis submitted in partial fulfillment of the
requirements for the degree of
Master of Science in Electrical Engineering
Department of Electrical Engineering

Shawana Tabassum, Ph.D., Committee Chair College

of Engineering

The University of Texas at Tyler
November 2022

The University of Texas at Tyler
Tyler, Texas

This is to certify that the Master's Thesis of

NAFIZE ISHTIAQUE HOSSAIN

has been approved for the thesis requirement on

10 NOVEMBER 2022

For the Master of Science in Electrical Engineering

Approvals:

DocuSigned by:
Shawana Tabassum
AA11ECFB133F4AF...

Thesis Chair: Shawana Tabassum, Ph.D.

DocuSigned by:
101C1CC8E9EC4E2...

Member: Prabha Sundaravadivel, Ph.D.

DocuSigned by:
Alwathiqbellah Ibrahim
3A3F3DF38EA844C...

Member: Alwathiqbellah Ibrahim, Ph.D.

DocuSigned by:
Hassan El-kishky
7E4401EB0BCF49D...

Chair, Department of Electrical Engineering

DocuSigned by:
3E50E32BE8F046A...

Dean, College of Engineering

Acknowledgments

All praise is due to God, who blessed my career with success. I would like to express my deepest appreciation and gratitude to my supervisor and committee chair, Dr. Shawana Tabassum for the continuous support. She continually conveyed a spirit of adventure and challenge, assistance and teaching. Without her care and guidance, nothing of this thesis would be possible.

It is a great pleasure to thank my committee members, Dr. Prabha Sundaravadivel and Dr. Alwathiqbellah Ibrahim, who supported and guided me with their insightful knowledge throughout my thesis. Also, my deepest gratitude goes to my mother and father for their everlasting care and support, prayers, and continuous encouragement.

In addition, I would like to thank my fellow labmates, Tanzila Noushin, Alina Nietsche Pereira, Angel Perez, and Francisco Perez for the stimulating research environment and all the enjoyment we had. Finally, I am genuinely appreciative to my friends, Vivek, Suwarna, Zabi, Carlos, and Rudy for their valuable advises, assistance, and time to push my career forward.

Table of Contents

List of Tables

List of Figures

Abstract

This thesis reports PlantFit: a research and development project that is intended to develop wearable sensors for plants. Plants are responsible for providing food, fiber, fuel, and fodder to the society. To overcome the problem of a limited land base, a more efficient farming approach needs to be developed, and thus precision farming is required. Precision farming would entail personalized healthcare in plants. When the plant is under any stress, the productivity declines. Plants release phytohormones, also known as early responders, in response to these stressors. The key crop phytohormones that respond to environmental stresses include salicylic acid (SA), indole-3-acetic acid (IAA), and ethylene (ET). While SA and IAA are liquid phytohormones, ethylene is a gaseous phytohormone. In this research, we have developed wearable sensors to detect SA, IAA, and ethylene phytohormones at different parts of plants such as leaf, stem, and fruit. The sensors are tested under different physical conditions, and it was found that the sensor response is reliable with a coefficient of variance of less than 5%. The developed sensor shows a high degree of sensitivity and selectivity. The sensor was deployed in live plants to measure hormone levels in real-time. The sensors will find a widespread use and will be useful in measuring plant stress early and in real-time, which will help farmers in taking immediate measures to reduce stress-induced yield decline. In addition, biologists can use the sensors to develop plant species that can cope with adverse environmental conditions such as drought and flood.

Chapter One

Introduction

Plants play a critical role in preserving ecosystem and preventing climate change by maintaining carbon cycle and water balance [1]. In fact, crops provide food which is associated with food security and nutrition for the society [2]. In recent years, transgenic crops, preservation of biodiversity, and sustainability in agriculture are adopted to cope with unprecedented economic and population growth. However, almost 690 million people fell in the state of hunger in 2019 and this number was 10 million more compared to 2018 and 60 million more compared to 2014. In addition, food price has experienced substantial instability in the recent years due to the COVID-19 outbreak [3]. Additionally, food security is challenged significantly by climate change such as natural disaster and extreme weather conditions [4] because they contribute to several contagious plant diseases. Because of biological and environmental stresses on plants, the crop productivity declines, which causes agricultural losses [5]. To be more specific, the biological stressors include pathogens [6-8] and pests attack [9], while the environmental stressors include flood [10], drought [11], heat wave [12] and icing [13]. These stressors are the main reasons for the deterioration of the plant health and losses in the productivity.

Various technologies have been employed to detect crop stresses including proximal optical sensor for monitoring N_2 deficiency [14], image-based plant disease detection [15] and smartphone-based techniques [16]. Although these techniques have proven their efficacy, they are not suitable for field applications because of lacking discrete monitoring capability, lower sensitivity and specificity, and transformation and reconstruction complexity. Remote sensing is an alternative methodology to conduct plant health monitoring [17]. Another very effective and promising approach of plant health monitoring is

electrophysiological detection of water stress and plant rhythm [18]. However, very few sensing technologies have been reported for personalized monitoring of biotic and abiotic stresses in plants.

Although wearable sensing technology has been used to enhance quality of life in humans by health monitoring [19-24], personalized diagnosis of health conditions [25-31], and human machine interface (HMI) [32-35], the technology is heavily unexplored in agriculture. To date, very few sensors are reported for plants [36]. Sensors can be placed in different plant organs including stem and leaves [37, 38]. Different organs of the plant serve different purposes and hence, multiple sensors are needed for monitoring varying physiology of plants. For instance, the primary function of roots is to collect water and various nutrients while the role of stem is to transport the water and nutrients to the leaves [38-39]. In addition, various gas exchanging mechanism such as the emission of volatile organic compounds, CO_2, O_2 and water vapor is primarily handled by small pores in leaves known as stomata [40,41]. Thus, to monitor plant health, various parameters need to be measured and analyzed. Plants release phytohormones in response to various abiotic and biotic stress conditions. Thus, the levels of these phytohormones, such as salicylic acid (SA), indole-3-acetic acid (IAA) and ethylene (ET), indicate and quantify the level of environmental stresses on plants. In addition, continuous monitoring of these phytohormones will allow personalized treatment for plants. [42].

In summary, we report a wearable sensor suite that monitors plant's fitness under various stress conditions. In the future, these stress levels will be reported to existing agricultural equipment to automate precise and efficient use of resources (e.g., nutrients, water, and pesticides).

Chapter Two

Overview of the Thesis

This section first provides a review of previous research, then defines the problem statement and finally reports our contribution to solve the problem.

2.1 Literature Review:

Considering the available sensing methodologies, electrochemical detection is a promising technique for the detection of signaling phytohormones in live plants. Electrochemical sensing is more favorable because of several aspects including the reliability, repeatability, accuracy and controlled sensitivity. In addition, the ease of preparation of the electronics at low cost with higher response time makes the electrochemical techniques stand out from other techniques [43]. Guided by these aspects, we have implemented electrochemical sensor-based phytohormone detection. We used functional nanomaterials to increase the analytical performance of the electrochemical biosensors [44]. The electrocatalytic capability of conductive materials was combined with redox reactivity of carbon-based nanomaterials [45, 46].

Recently, paper based electrochemical sensors are reported to detect hydrogen peroxide and salicylic acid in tomato plants infected by certain pathogens (Botrytis cinerea) [47, 48]. Salicylic acid helps in plant defense and immunity [49-51]. However, the detection mechanism involves punching a hole in the leaf. Other existing technologies involve extracting and cutting leaves, which incurs a destructive sample collection procedure [52].

Another research group proposes insertion of a sensor inside the fruit so that real time measurement of metabolites is possible; more specifically real time tryptophan is detected which plays a vital role in

biosynthesis of auxins [53-55]. A stainless-steel wire-based electrode is developed with significantly lower limit of detection of 43 pg/mL to detect IAA in live plants [56]. However, these electrochemical sensors are made of a wire that damages the plant tissue and hence are not practical for long-term detection in plants. Very few research projects have been reported to detect gaseous phytohormones, such as ethylene (ET). The selective detection of ET is challenging because of its small atomic size and nonpolar behavior. One notable work to detect ethylene involves single walled carbon nanotube with copper complex coating [57]. But the sensor is made on a rigid glass slide which is difficult to place on plants. This research addresses these issues and proposes a scheme for in situ sensing of phytohormones in live plants.

Phytohormone controls the plant physiology such as gas control rate including CO_2 intake as well as O_2 releases and utilization of nutrient which in turn drives transpiration [58-59]. These phytohormones such as SA and IAA control the plant metabolism rate. It is known from the previous literature that with increasing metabolism, the rate of transpiration is higher i.e., the translocation of water to the leaf is higher [60, 61]. The phytohormones such as SA, IAA, and ethylene indicate plant's metabolism rate which in turn can detect plant stress [62-65]. Previously no work has been done to detect the multiplexed phytohormones in live plants to detect the plant stress as well as water translocation simultaneously.

2.2 Problem Statement

The detection of phytohormone is challenging as it involves the detection of chemical compounds. One solution is to measure the phytohormones with an electrochemistry-based sensor. However, the conventional electrochemical sensors are made on rigid ceramic surfaces or paper-based substrates [66]. The ceramic substrate is not suitable for plants as they are not flexible. The problem with paper-based sensors is reliability, as the quality of the paper substrate tends to decrease when they are in contact with water or liquid. As SA and IAA are liquid phytohormones, a flexible

electrochemical sensor is needed with reliable sensing performance over time. Another challenge is the liquid phytohormones are released inside the plant tissue and are not available from outside. In summary, a multiplexed sensor suite must be developed that can detect phytohormones noninvasively or in a minimally invasive approach, has a reliable sensing performance over time, and is lightweight so that it can be easily mounted on leaves and stem.

2.3 Contribution

There are three major contributions of this research work. Firstly, for the first time, an electrochemistry-based flexible sensor has been developed that shows a high degree of reliability. Secondly, minimally invasive microneedle-based electrochemical sensors are developed to detect plant phytohormones for the first time. Finally, a flexible and microneedle-based hybrid sensor suite has been developed for special parts of the plant, such as fruits and vegetables that tend to have a very irregular surface.

‘

Chapter Three

Wearable Sensor Fabrication

At the beginning of this thesis project, a planar sensor was implemented. Next, to improve the efficiency, a microneedle-based sensor was implemented and finally a hybrid sensor was developed for site-specific applications.

3.1 Flexible Sensor

In this section the development of phytohormone sensors in a flexible sheet will be discussed. The main purpose of making the sensor patch is to detect the key phytohormone, SA. The electrochemical sensor consists of three electrodes, namely working electrode, counter electrode, and reference electrode. The electrodes are made on a polymer substrate, which is flexible in nature [68, 69]. The polymer sheet is 125 micrometers thick. Another flexible patch contains a strain sensor for stem diameter measurements. Figure 3.1 shows the step by step procedure to fabricate the sensor and Figure 3.2 shows the chronological order of fabrication of the strain sensor.

Briefly, the sensor structure (two dimensional) is designed in AutoCAD Fusion 360. The design is exported to a cutting machine where polymer sheet is covered with a transfer tape, which is removed after transferring the design to the polymer sheet. The speed, force and blade angle are optimized during each cutting. In this sensor fabrication, speed, force and angle were 4.1N, 97mm/s, and 30°, respectively.

The strain sensor is composed of interdigitated electrodes that are coated with graphene ink (annealed at 100°C for 10 minutes). The design is made in AutoCAD followed by feeding that to the cutting machine. The force, speed and blade angle are optimized to 4.05N, 98mm/s and 30°, respectively.

The SA sensor's working and counter electrodes are made with graphene ink and annealed at 300°C temperature for 15 minutes. The strain sensor electrodes are interdigitated and made with the same procedure as the working and counter electrodes of the SA sensor. The reference electrode of the SA sensor is made with silver/ silver chloride paste. The silver/silver chloride paste is applied over the selected regions and cured at 80°C for 20 minutes. The brief fabrication procedure of making SA and strain sensors is illustrated in Figure 3.1 and Figure 3.2.

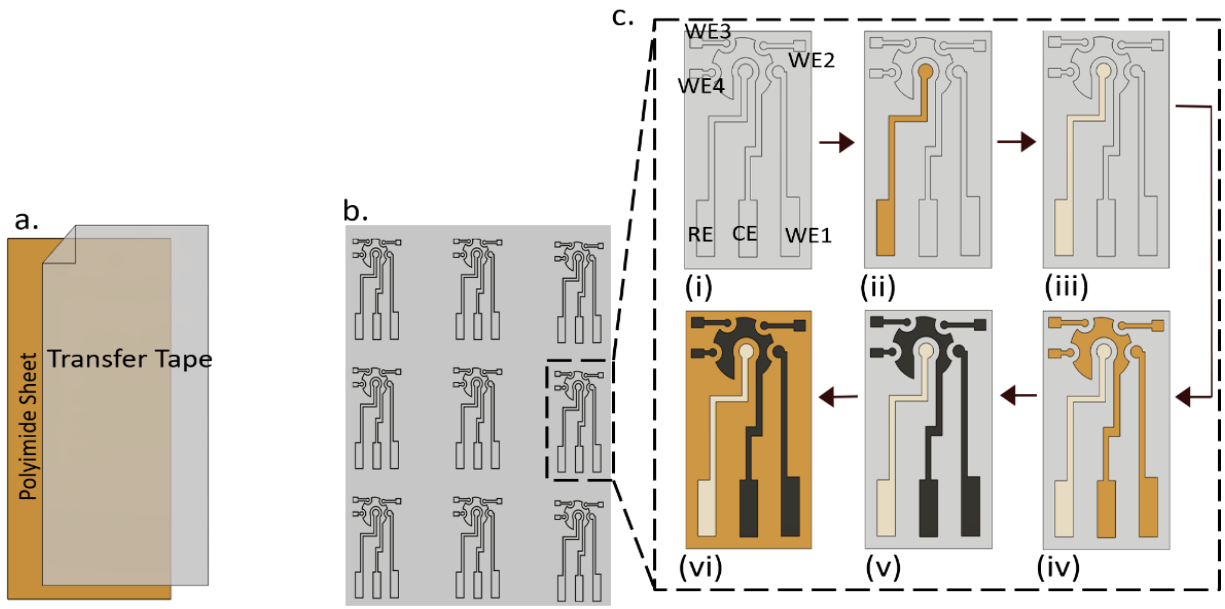

Figure 3.1: Schematic illustration of the sensor fabrication process. (a) A transfer tape was attached to the polymer sheet and loaded on the cutting machine. (b) An array of patterns was cut on the tape. (c) Steps of screen-printing [74].

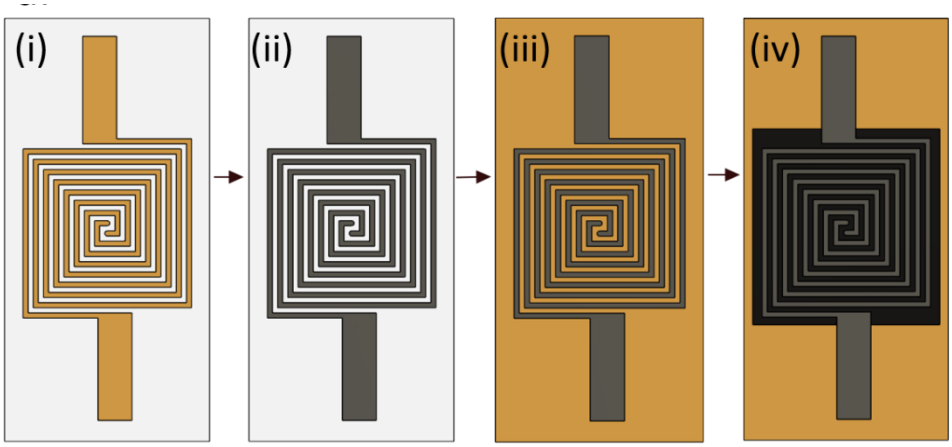

Figure 3.2: Process flow for the strain sensor: i) the transfer tape is removed from the cut regions, ii) graphene ink is applied over the patterned region and cured, iii) the remaining transfer tape is peeled off, iv) drop-casting of rGO dispersion [75].

3.2 Microneedle Based Sensor

A microneedle-based stem sensor is developed for the detection of SA and pH, while a microneedle-based leaf sensor is developed for SA, IAA, and temperature detection. The pH and temperature sensors are incorporated with the phytohormone sensors because they also play an important role in detecting plant stress. The fabrication procedure of these two systems is described in the following paragraphs.

A microneedle-based stem sensor comprising SA and pH sensors on a single chip is shown in Figure 3.3. The novelty of this sensor relies on the development of microneedle sensors for the stem for the first time to detect the stress related phytohormones. The SA sensor is based on three electrodes: working electrode, counter electrode, and reference electrode. One microneedle is made for each electrode so that less damage is caused to the plant. The microneedle is made with 3D printing. After the needles are printed, they were cured in ultraviolet light with a constant rotation

for 70 minutes. The needles are pyramidal shaped with a square base. The height and base width of the pyramidal shaped microneedles are 800 micrometers, while the tip angle is 30 degree. The reason for choosing the 30-degree tip angle is to penetrate the stem easily. The working electrode of the pH and SA sensors as well as the counter electrode of the SA sensor is coated with graphene ink and cured at 300°C for 15 minutes. Finally, the reference electrode is made with silver/silver chloride paste which is annealed at 80°C for 30 minutes. The step-by-step fabrication procedure is shown in the following Figure 3.3.

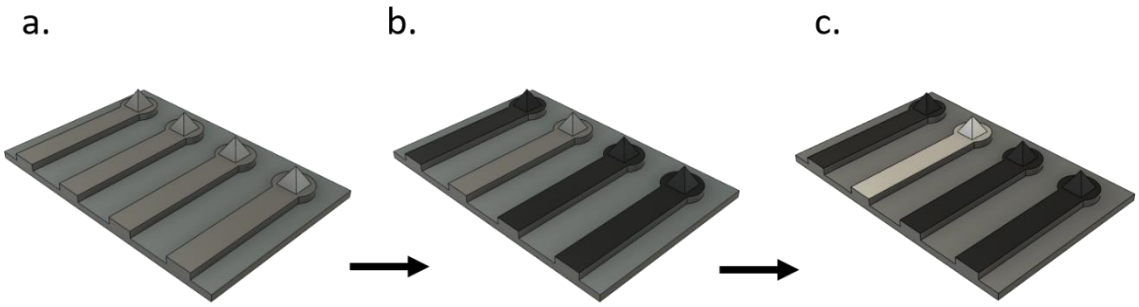

Figure 3.3: (a) The microneedle structure is made with 3D printing; (b) the needles are coated with graphene ink; (c) the reference electrode is made with silver/silver chloride ink [76].

The second microneedle sensor is implemented for monitoring SA, IAA and temperature in plant leaves. Each electrode is composed of an array of microneedles. The reason to make the microneedle array is to increase the surface area as leaf has a larger area. Similar to the stem microneedle sensor, the leaf microneedle sensor has a two-electrode temperature sensor incorporated with it. This microneedle structure is also made with a 3D printer. The base dimension of the needle is the same as the previous needle, but the height of the needle is 2000 micrometer. As the height increased, the tip angle also increased to 60°. The working electrode of the temperature, SA, and IAA sensors are made with graphene ink and cured at the same

condition as before. The reference electrode is common for the SA, IAA and temperature sensors. The reference electrode is made with silver/silver chloride paste.

The graphical illustration of the leaf microneedle sensor is given in Figure 3.4.

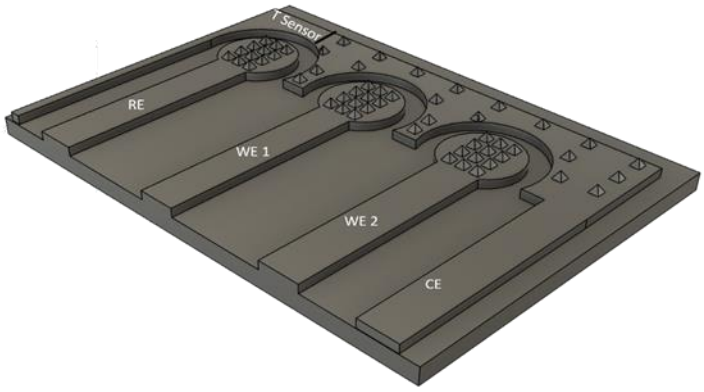

Figure 3.4: Microneedle based sensor for leaf [78].

3.3 Hybrid Sensing Approach

The hybrid sensor is comprised of SA, IAA, ethylene, and pH sensors on a single device. This microneedle-based hybrid sensor is made for fruit ripeness measurement. The sensor is composed of one array of microneedles for the SA working electrode and one array of microneedles for the IAA working electrode. Both SA and IAA sensors have a common counter electrode and a common reference electrode. The reference electrode is also common for the pH sensor. The microneedle structure is made in such a way that it housed a planar ethylene sensor and a gas accumulation chamber. The base and width of the microneedles are fixed at 800 micrometers, while the tip angle is fixed at 60°. The ethylene sensor is made according to the previously mentioned process with slight modification. The ethylene sensor is made on a nafion membrane using screen printing [67, 68]. A transfer tape is attached over the nafion membrane and then screen-printed with conductive electrodes. Figure 3.5 shows the step by step procedure to fabricate the sensor suite.

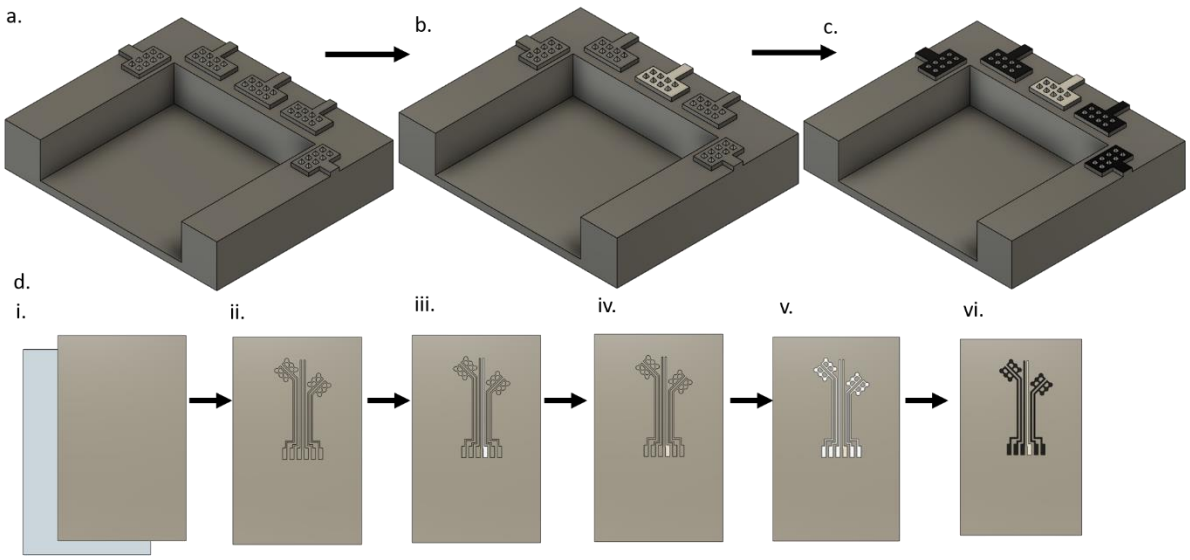

Figure 3.5: Step-by-step fabrication of the electrodes. (a-c) The 3D printed microneedle electrodes. (d) Screen printing of ethylene sensor [79].

This sensor is called hybrid because it implements both planar and microneedle-based approaches. Hybrid sensors are better compared with only planar or only microneedle-based sensor. This is because a hybrid sensor is capable of detecting gaseous and liquid phytohormones simultaneously. Previously, no sensor suit shows the detection of liquid and gaseous phytohormones.

Chapter Four

Synthesis of Chemical Coatings, Sensor Characterization, and Calibration

In this chapter, the synthesis of chemical coatings, characterization and calibration of sensors are described.

4.1 Coating Synthesis

4.1.1 A composite coating of copper metal organic framework-carbon black-Nafion for Salicylic Acid sensing

Salicylic acid detection is done by a copper-based metal organic framework. The synthesis process of the copper metal organic framework is quite complex, and the detailed process is described in a previous report [69]. The procedure is briefly explained here. At first, an anhydrous solution of dimethylformamide (DMF) is added to CH_3-CH_2OH. Next, the resulting solution in made uniform via a centrifuge. Once a uniform solution is achieved, polyvinyl pyrrolidone (PVP) is added to the mixture. Next, coper nitrate and 2-aminobenzene-1,4-dicarboxylic acid are added to the DMF solution. The resulting mixture is centrifuged to achieve a high degree of uniformity. After that the solution is heated so that the reaction takes place. The resulting product is precipitated, which is collected and then dissolved in the fresh DMF solution. The final DMF solution is heated again overnight. The final precipitate is collected and heated to remove the water content. This product is the desired copper metal organic framework (CuMOF).

The CuMOF is then mixed with carbon black at a certain ratio to get the best result. A small amount of nafion is added to the solution to complete the coating preparation. The resulting solution is drop casted over the bare sensor for selective detection of SA.

4.1.2 A composite copper complex (I)-single-walled carbon nanotube coating for ethylene sensing

We followed the recipe in [56] to prepare the copper complex coating. In summary, sodium borohydride is added to [3,5-(CF3)2pyrazol-1-yl] in an inert medium. Kerosene was used to facilitate the dispersion and prevent any agglomeration. Temperature was ramped gradually and then kept constant for several hours. Then the solution containing beaker was partially submerged into organic oil and heated continuously and uniformly. A heat gun was used to evenly heat the solution to prevent any agglomeration of the intermediate product. Then the heat gun was turned off and diethyl ether was added to filter out the product from the reagent. The product was characterized using nuclear magnetic resonance (NMR) spectroscopy and the results are discussed later in Section 4.2. The chemical formula of the expected product is $Na[HB(3,5\text{-}(CF_3)_2\text{-}pz)_3]$. Next, in a separate container, HPLC grade toluene and copper(I) trifluoroethane sulfonate benzene complex were mixed and the resulting solution was mixed vigorously to achieve uniformity. In this solution the previously synthesized product was added and stirred. Finally, the solution was filtered using a fine filter paper to get the desired copper complex powder.

Finally, to prepare selective coating for the ethylene sensor, single walled carbon nanotube was dissolved in the mixture of 1,2-dichlorobenzene and toluene (which was made uniform). In this homogeneous solution, the as prepared copper complex powder was added, and the solution was made uniform. The resulting solution was drop casted over the ethylene electrodes and dried at room temperature.

4.1.3 Reduced graphene oxide coating for strain sensing

The strain sensor is prepared using reduced graphene oxide (rGO). rGO is dispersed in N-methyl-2-pyrrolidone (NMP). Different concentrations of rGO is made to have an optimized solution. It should be mentioned that a long duration of sonication was required to prepare the uniform dispersion of rGO. Finally, the dispersion was used as a coating.

4.1.4 Polyaniline based pH sensing

The pH coating is made according to the previously mentioned procedure [70]. At first polyaniline solution is made. Then cyclic voltammetry is applied between the electrodes of the pH sensor. A nanofiber is created which is sensitive to hydroxyl ion.

4.1.5 Gold Doped Graphite Hydrogel for IAA detection

The IAA coating is based on preparation of Gold nanoparticle doped Graphite Hydrogel (AuNP-GH). The detailed preparation procedure is discussed in the literature [71]. In short, graphene oxide solution is made where one fourth volume of hydro tetrachloro gold and triethylenetetramine are added and then after making the solution uniform, the resulting solution is autoclaved overnight at high temperature. The resulting hydrogel is collected and then freeze dried to make a power and then used as the coating over the IAA sensor electrode.

4.2 Coating Characterization

To characterize the coating, several methods are utilized. Fourier Transform Infrared Spectroscopy (FTIR) is used to characterize the CuMOF coating (Figure 4.1a). The peaks between 3550 and 3390 cm^{-1} wave numbers refer to the symmetric stretching of amino groups originating from 2-aminobenzene-1,4-dicarboxylic acid. The stretching peak at a wavenumber of 2950 cm^{-1} appears

because of the presence of hydroxyl groups that mainly originate from ethanol. The FTIR characterization of CuMOF coincides with the previous report [72]. Further, the CuMOF surface is analyzed via scanning electron microscopy (SEM) (Figure 4.1b).

The copper complex is characterized with NMR spectroscopy (Figure 4.1c). The most crucial step of preparing the copper complex coating is the product Na[HB(3,5-$(CF_3)_2$-pz)$_3$]. The NMR spectra shows the presence of this product in the diethyl ether mixture. The SEM analysis of the final coating implies that the mean diameter of the nanoparticles is almost 10nm (Figure 4d).

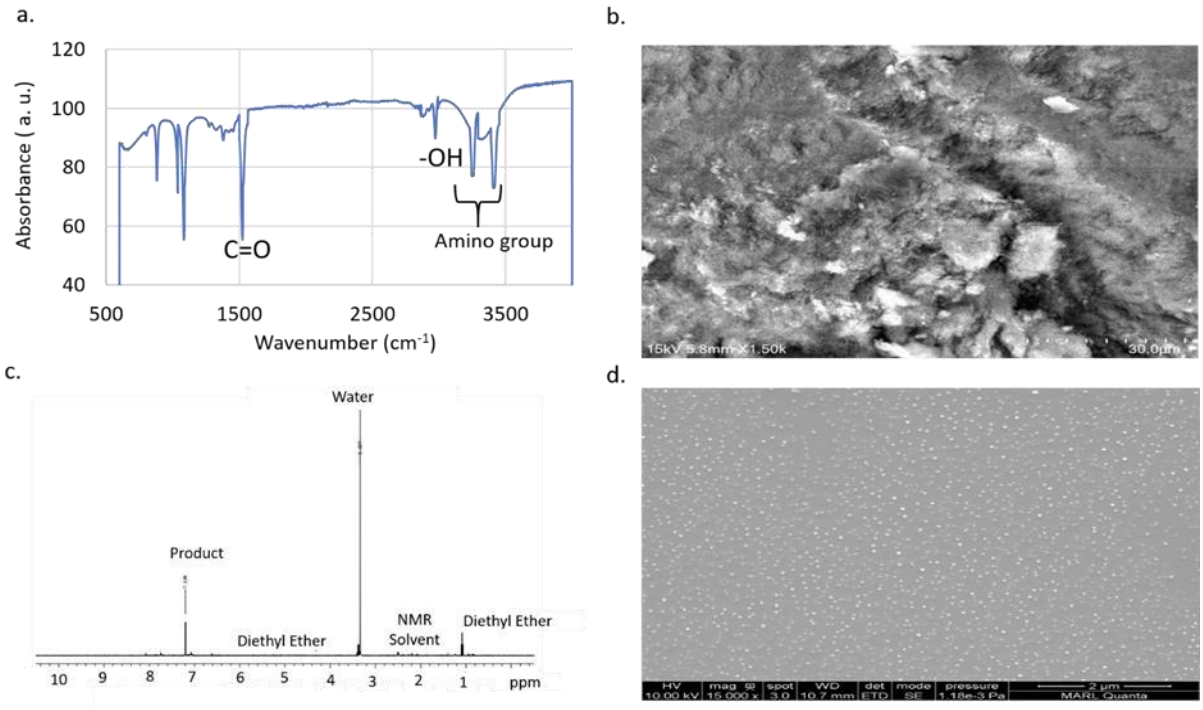

Figure 4.1: (a) Characterization of CuMOF using FTIR. (b) SEM image showing the morphology of the CuMOF/CB/nafion coating over the working electrode of the SA sensor. (c) NMR spectroscopy of the ether mixture of Na[3,5-$(CF_3)_2$-pz]. (d) SEM image of copper complex nanoparticles over the working electrode of the ethylene sensor.

The UV Vis spectra of the AuNP-GH is shown in Figure 4.2 where the gold peak and C=O bond are visible.

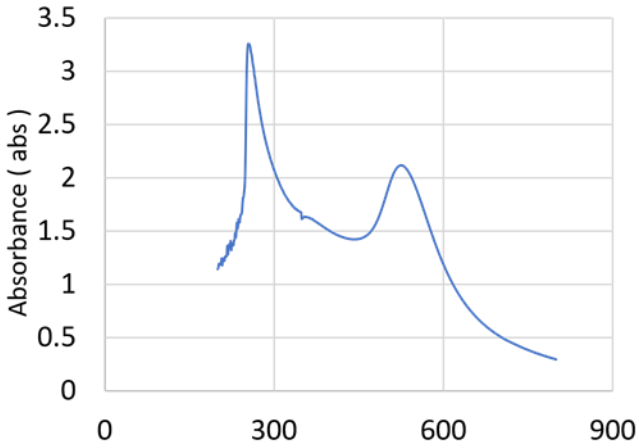

Figure 4.2 *Characterization of AuNP-GH with UV-Vis* [78].

4.3 Sensor Calibration

The electrochemical sensors are calibrated using electrochemical techniques such as differential pulse voltammetry (DPV) and cyclic voltammetry (CV). The DPV technique is run from 1.0V to 1.5V with a step voltage of 0.01V. The scan rate is fixed at 10mV/s. To calibrate the SA sensor, eight different concentrations are chosen, such as 1 µM, 10 µM, 100 µM, 200 µM, 400 µM, 600 µM, 800 µM and 1000 µM of SA. The DPV spectrum consists of two major peaks. The first peak is the result of the reduction of copper ion in the CuMOF coating while the second peak is due to the oxidation of SA. The carbon black works as a functional material. It is noteworthy to mention that the first current peak decreases while the second peak current increases with increasing SA concentration. In addition, there is a significant potential difference between the copper peak and the salicylic acid peak. Hence the ratio of the two peak currents was utilized for calibration. Figure 4.3a and 4.3b show the DPV spectra and the corresponding calibration curve for the SA sensor, respectively.

Cyclic voltammetry is utilized to calibrate ethylene sensor. The CV is performed from -0.2V to 0.5V at a scan rate of 50mV/s and Estep of 0.01V. Seven different concentrations of ethylene (1ppm, 10 ppm, 30 ppm, 50 ppm, 75 ppm, 105ppm, and 115 ppm) are used for calibration. When ethylene is absorbed by the copper complex coating, a complex is formed that reduces the conductivity of single walled carbon nanotube. Due to this phenomenon, the current decreases as the concentration of ethylene increases. The current value is plotted against logarithmic value of the ethylene concentration in ppm which gives a linear response (Figure 4.3c and 4.3d).

The strain sensor is resistive in nature. The sensor is calibrated using an LCR meter. The strain sensor is calibrated for various angles of curvature. The equation that relates the angle of curvature and radius is given below.

$$\theta = \frac{360\,S}{2\pi r}$$

Where s, r and θ represent arc length, radius, and angle of curvature, respectively. The calibration curve of the strain sensor is shown in Figure 4.4.

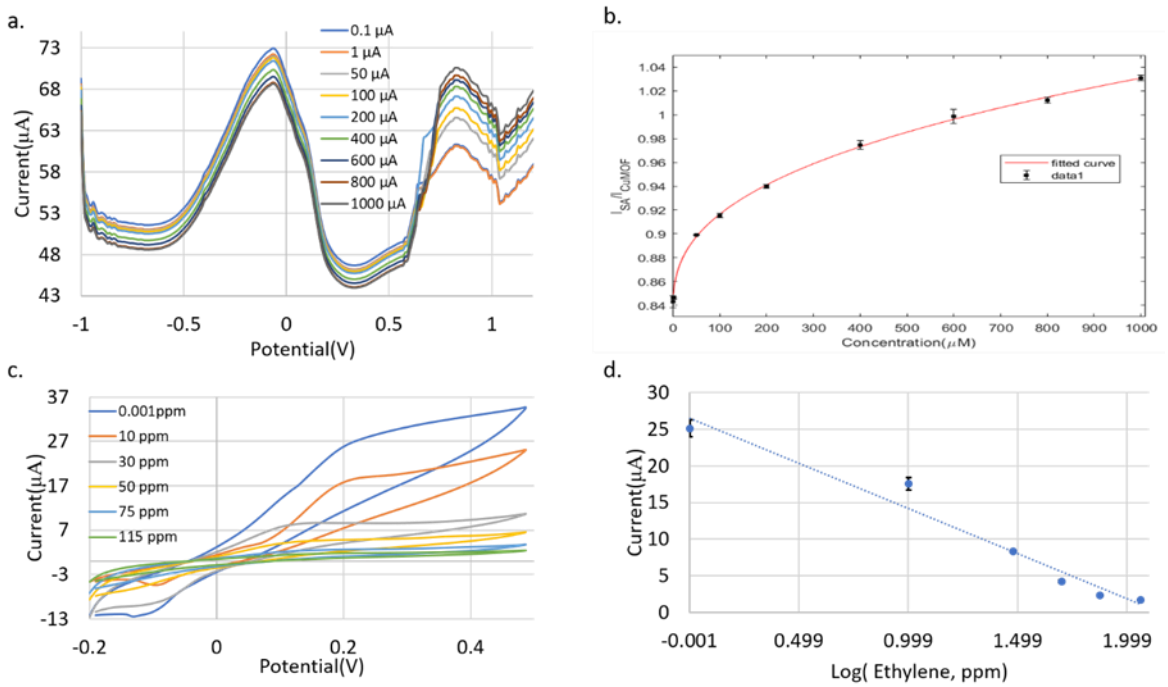

Figure 4.3. (a) DPV responses for different concentrations of Salicylic Acid. (b) Calibration curve of SA sensor indicating the I_{SA}/I_{CuMOF} vs. concentration. (c) CV responses for different concentrations of ethylene. (d) Calibration of ethylene sensor representing the peak current vs. logarithm of the concentration.

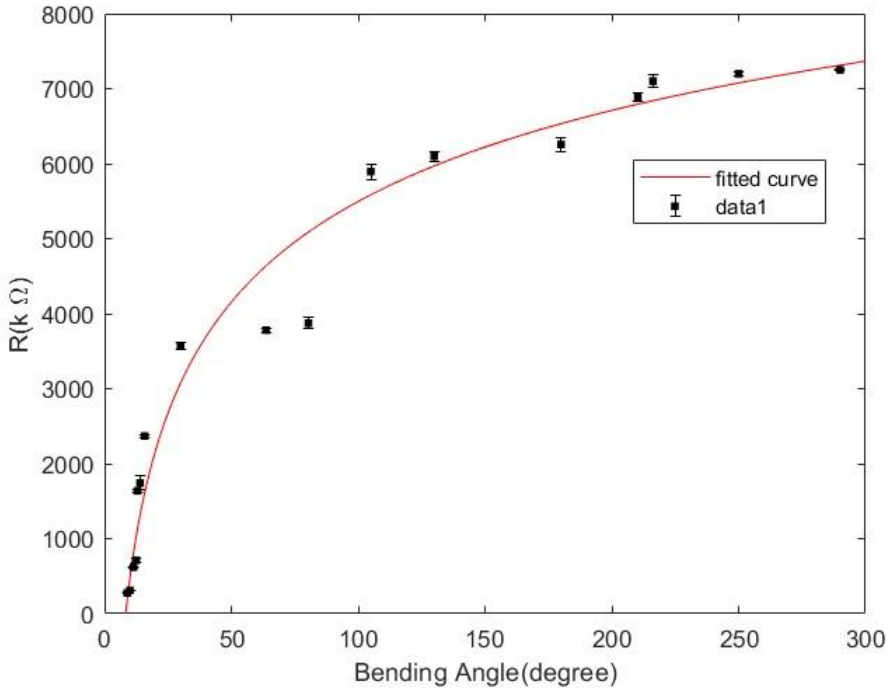

Figure 4.4: Calibration curve of the strain sensor.

4.4 Sensitivity and Limit of detection (LOD) analysis

The sensor response for unit change in analyte concentration or any physical parameter is referred to as sensitivity. When the sensor has a linear response, the slope of the calibration curve is called sensitivity. The sensitivity calculation is different for a non-linear sensor. We observed a non-linear response for salicylic acid and strain sensors, which may be due to the material property. The calibration curves for salicylic acid and strain sensors are fitted with power series curves. The derivative of the power series curve is taken, and two sensitivity values are calculated. The preferred approach is to measure the sensitivity at low and high concentration/strain values [74]. Briefly, from the fitted curve:

$$S_y|_x := \frac{dy}{dx} = abx^{b-1}$$

The lowest amount of analyte or any physical parameter that can be detected by the sensor consistently and accurately is known as the limit of detection (LOD). For SA, temperature, and strain sensors, the limit of detection is calculated by using the following equation.

$$LOD = \frac{3^{*}\ std.\ dev.}{Sensitivity}$$

LOD for the ethylene sensor is calculated by the following equation [73],

$$LOB = mean\ of\ signal\ (blank\ sample) + 1.645\ (std.\ dev.\ of\ blank\ sample)$$

$$yLOD = LOB + 1.645\ (std.\ dev.\ of\ target\ at\ low\ \ concentration\ )$$

$$LOD = \frac{yLOD - intercept}{slope}$$

Table 4.1 Summary of sensitivity and limit of detection (LOD) for nonlinear sensors.

Sensor	Equation	Sensitivity (low concentration)	Sensitivity (high concentration)	Limit of detection
SA	$I_{SA}/I_{CuMOF}=0.0143(conc.)^{0.3787} + 0.8346$	0.002264 μM^{-1} (at 0.1 μM)	7.409 X 10^{-5} μM^{-1} (at 1000 μM)	0.644 μM
Strain	$R=0.000248\theta^{0.1442} + 18260$	1.5935 X 10^{-6} kΩ/°	1.006 X 10^{-8} kΩ/°	9.3211°

Table 4.2 Summary of sensitivity and limit of detection (LOD) for linear sensors.

Sensor	Equation	Sensitivity	LOD
Ethylene	$I= -17.073\ (conc.) + 34.635$	17.073 μA/log(ppm)	0.6089 ppm
Temperature	R/Ro=0.098 (temp.) +1.17313	0.0098/°C	10.5478°C

4.5 Drift Analysis

The hormone sensors (SA and ethylene) are tested for drift. Drift analysis is done to help determine whether the sensor is capable of continuous operation and if so, how much deviation can be found at different time points given that the physical conditions are the same. Every sensor has gone through long term (12 h) drift testing for a constant concentration of phytohormone. Figure 4.5 shows the drift analysis of the hormone sensors. The sensors demonstrate less than 1% coefficient of variance over 12 hr.

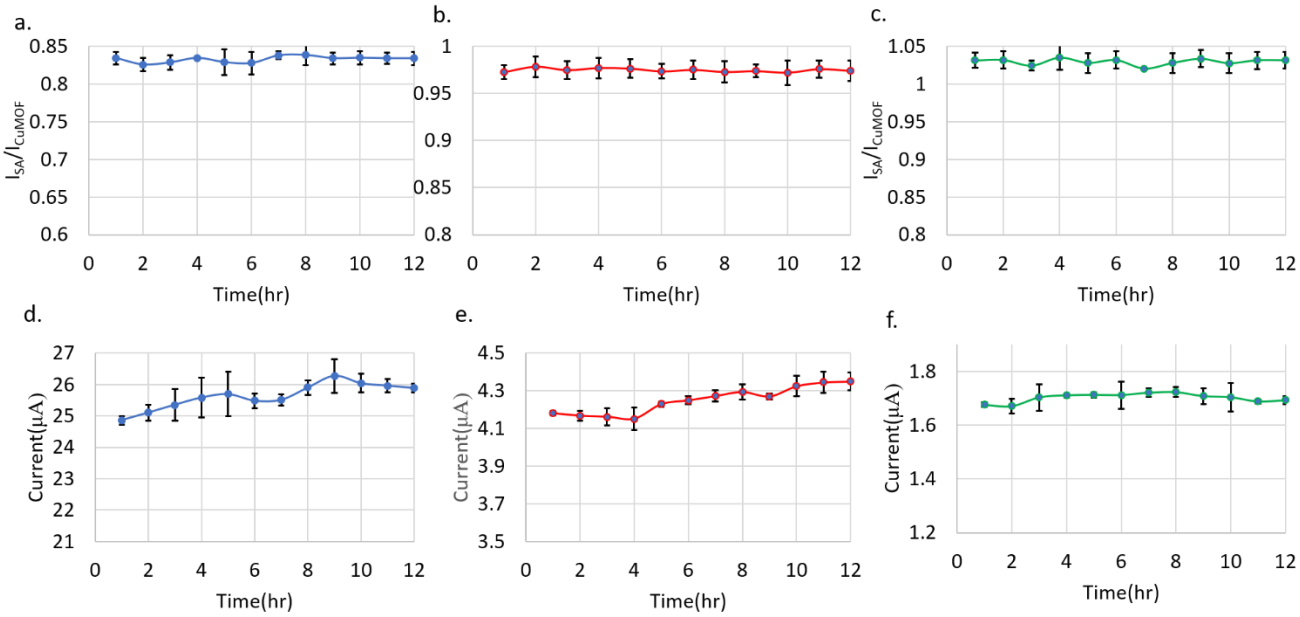

Figure 4.5. Twelve-hour drift response of salicylic acid sensor for 0.1μM (a), 400 μM (b) and 1000 μM (c) concentrations. Twelve-hour drift response of ethylene sensor for 0.001ppm (d), 50 ppm (e) and 115 ppm (f) concentration.

4.6 Selectivity Analysis

The ability of the sensor to detect the target molecule in presence of any unwanted species is known as the selectivity of the sensor. One of the most important criteria before deploying the sensor especially electrochemical sensors in field is to check whether the sensor is selective or not.

Selectivity test is done for both salicylic acid and ethylene sensors (Figure 4.6). For salicylic acid the tested solutions are: (i) 50 µM of glucose, (ii) 50 µM of sucrose, (iii) 50 µM of soluble starch, (iv) 50 µM of L-tryptophan, (v) 50 µM of L-cysteine, (vi) 50 µM of abscisic acid (ABA), (vii) 50 µM of gibberellic acid (GA), (viii) 50 µM of Jasmonic acid (JA), (ix) 50 µM of oleic acid (OA), (x) 50 µM of indole-3acetic acid (IAA), (xi) 50 µM of citric acid (CA), (xii) 50 µM of salicylic acid (SA), (xiii) a mixture of 50 µM glucose, soluble starch, L-tryptophan, L-cysteine, ABA, GA, JA, OA, IAA, CA each, (xiv) a mixture of 50 µM glucose, soluble starch, L-tryptophan, L-cysteine, ABA, GA, JA, OA, IAA, CA each, and 100 µM of SA, (xv) 900 µM of SA, and (xvi) a mixture of 50 µM glucose, soluble starch, L-tryptophan, L-cysteine, ABA, GA, JA, OA, IAA, CA each, and 900 µM of SA.

The relative signal strength is considered instead of the base current. The relative signal is defined as $\frac{Ra-Rb}{Rb}$, where Ra = ratio of hormone redox current and CuMOF current

and Rb =ratio of base current and CuMOF current. The relative signal analysis plot indicates superior selectivity of the SA sensor.

To evaluate the selectivity of the ethylene sensor, various gas mixtures were used: (i) 50 ppm of nitrogen (N_2), (ii) 50 ppm of methane (CH_4), (iii) 50 ppm of nitrous oxide (N_2O), (iv) 50 ppm of ammonia (NH_3), (v) a mixture of 50 ppm of N_2, CH_4, N_2O, NH_3 each, (vi) 10 ppm of ethylene, (vii) 115 ppm ethylene, (viii) a mixture of 50 ppm of N_2, CH_4, N_2O, NH_3 each, and 10 ppm of ethylene, and (ix) a mixture of 50 ppm of N_2, CH_4, N_2O, NH_3 each, and 115 ppm of ethylene. The difference of the current from the baseline is considered for selectivity analysis.

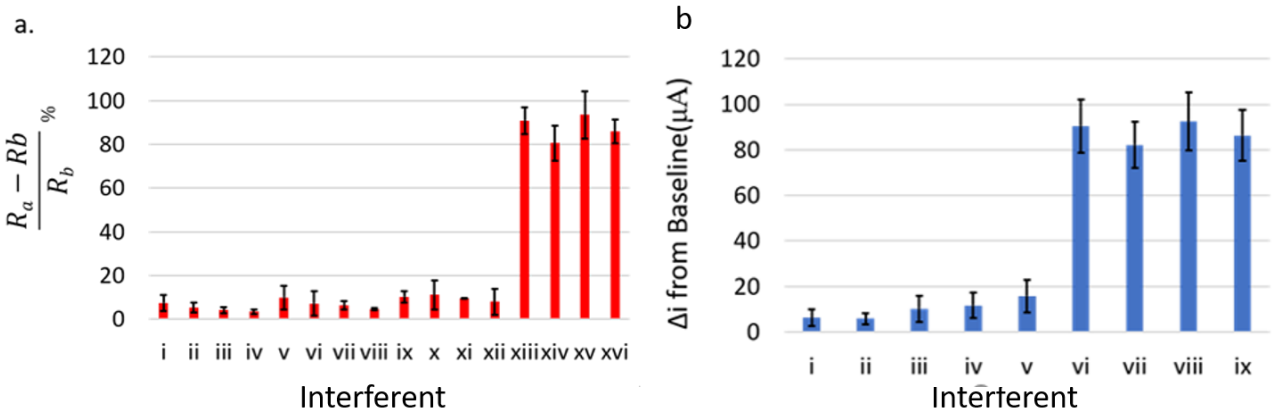

Figure 4.6. (a) Relative signal for different solutions introduced over the SA sensor surface, where i-xvi denote: (i)50 µM glucose, (ii)50 µM sucrose , (iii)50 µM soluble starch, (iv) 50 µM L tryptophan, (v)50 µM L cysteine, (vi)50 µM abscisic acid(ABA), (vii)50 µM gibberellic acid(GA), (viii)50 µM Jasmonic acid(JA), (ix) 50 µM oleic acid(OA), (x)50 µM indole 3 acetic acid(IAA), (xi)50 µM citric acid(CA), (xii)50 µM salicylic acid(SA), (xiii)mixture of 50 µM glucose, soluble starch, L trypan L cysteine, ABA, GA, JA, OA, IAA, CA each , (xiv)mixture of 50 µM glucose, soluble starch, L trypan L cysteine, ABA, GA, JA, OA, IAA, CA each with 100 µM SA, (xv)900 µM SA and(xvi) mixture of 50 µM glucose, soluble starch, L trypan L cysteine, ABA, GA, JA, OA, IAA, CA each with 900 µM SA. (b) Current(µA) Difference from the baseline for the ethylene sensor, where i-ix represents: (i)50ppm nitrogen(N_2), (ii) 50 ppm methane(CH_4), (iii)50 ppm nitrous oxide (NO), (iv)50 ppm ammonia(NH_3), (v) 50ppm of ethylene a mixture of 50ppm of N_2, CH_4, NO, NH_3 each, (vi)10 ppm ethylene, (vii) a mixture of 50ppm of N_2, CH_4, NO, NH_3 each with 10 ppm of ethylene(viii) 115 ppm ethylene and (ix) a mixture of 50ppm of N_2, CH_4, NO, NH_3 each with 115 ppm of ethylene [79].

4.7 Stability Analysis

In a real agricultural field, environmental factors are not controlled and the stability of the sensor in these cases must be evaluated. The salicylic acid and ethylene sensors show considerable stable response with less than 1% coefficient of variance over a week.

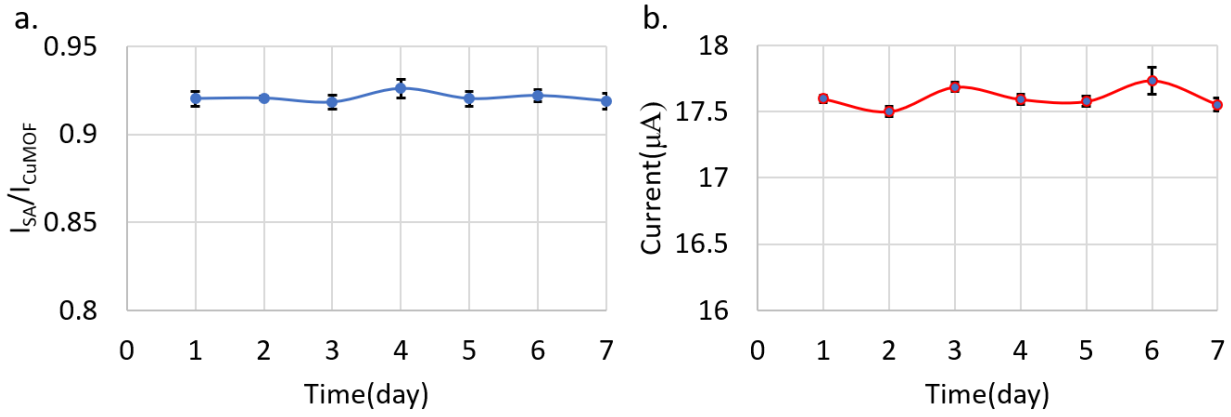

Figure 4.7. Stability Analysis of (a) salicylic acid (100μM) and (b) ethylene (10ppm) sensors.

4.8 System Development

A separate data acquisition unit was made for the strain sensor. The main processing unit of the data acquisition unit is MKR 1000 board. The MKR 1000 board has WiFi capability. The board is programmed to measure resistance with an auto-ranging function. The strain sensor is calibrated using cylindrical blocks. The block diagram and the corresponding circuitry are shown in figure 4.8 [74].

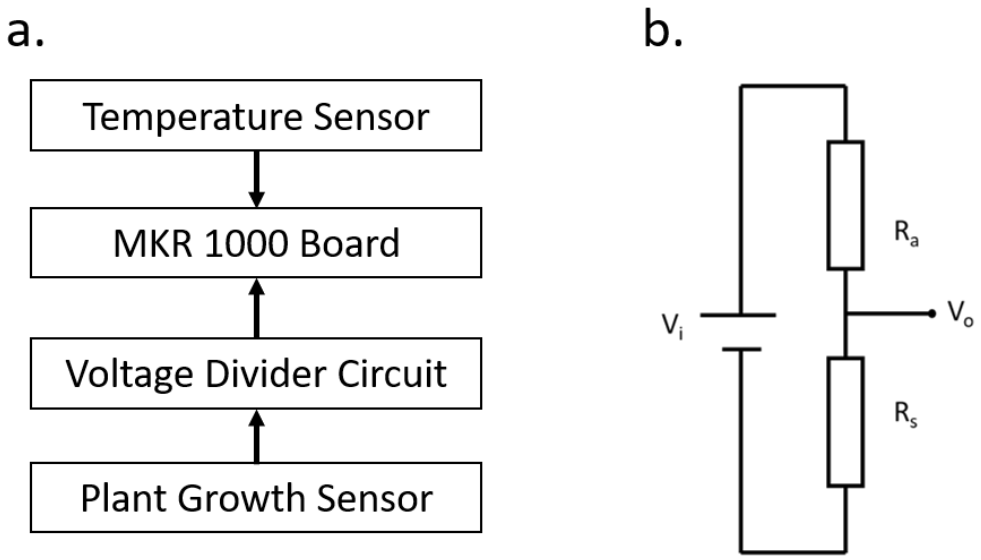

Figure. 4.8. (a) System architecture. (b) The voltage divider circuit wherein R_a is a variable resistor, R_s and V_0 are the resistance and the voltage across the strain sensor, respectively [74].

4.9 Real plant data collection

To perform in situ experiment, the flexible sensor is placed beneath the leaf of a bell pepper plant. Figure 4.9a shows the schematic and practical deployment of the developed flexible sensor. A 5 micrometers radius hole is punched on the leaf, and 20 microliters of buffer is applied. A spacer is placed between the sensor and the leaf so that the plants can transpire naturally. The spacer is made with a polymer sheet which has a thickness of 125 micrometers, while the radius of the sensor is 1.5 centimeters. The Differential Pulse Voltammetry (DPV) results of the stressed and unstressed plants are presented in Figure 4.9 b. The corresponding FTIR results are also included (Figure 4.9c). The salicylic acid concentrations measured with our sensor and FTIR technique are almost identical with a deviation of less than 2%. The ratio of the SA peak and the CuMOF peak for the stressed plant is higher (0.94319) compared with the controlled plant (0.9042) [75].

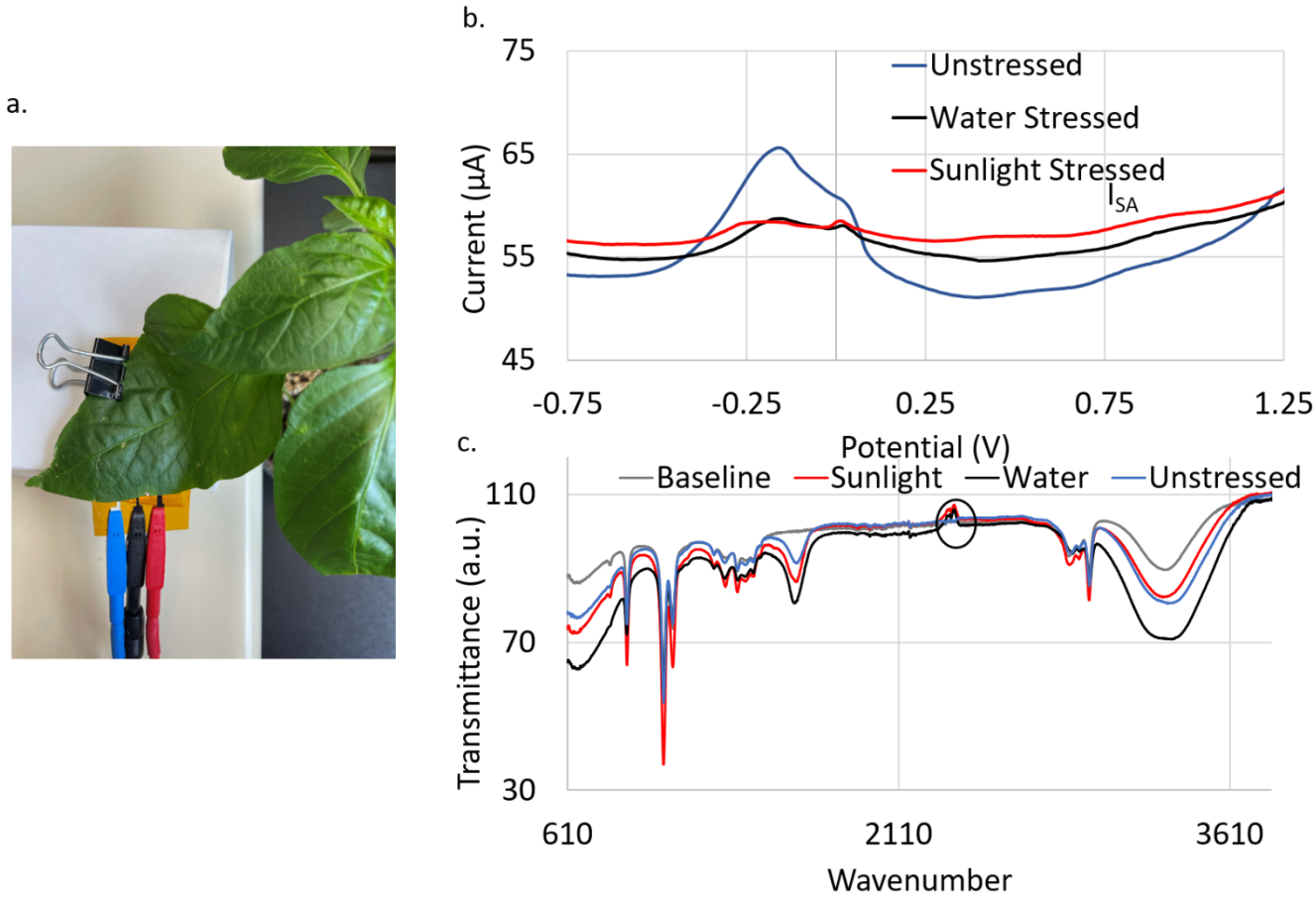

Figure 4.9: (a) Real-time SA measurements in the leaf.; (b) DPV and (c) FTIR responses for the sap collected from unstressed, water- and sunlight-stressed plants [75].

Chapter Five

Results of Microneedle and hybrid Sensor Analysis

5.1 Microneedle based stem sensor

The details of the microneedle-based stem sensor are described in our previous work [76]. The pH sensor is made along with SA sensor in this work. It is used to detect plant stress accurately. Figure 5.1 shows the pH sensor characterization and calibration plots, while Figure 5.2 shows the SA sensor response. Figure 5.3 represents the pH response of the SA sensor. At low pH when the medium is acidic, the SA sensor shows a higher peak current, I_{SA} due to electron affinity. However, at high pH when the medium is basic, I_{SA} is lower due to less availability of the electrons.

The SA level of the water stressed and unstressed plants is shown in the Figure 5.4a. With the increasing stress level on plants, the SA level also increases. Two different sensors at different stem positions of the same plant is placed and the corresponding results are shown in Figure 5.4b.

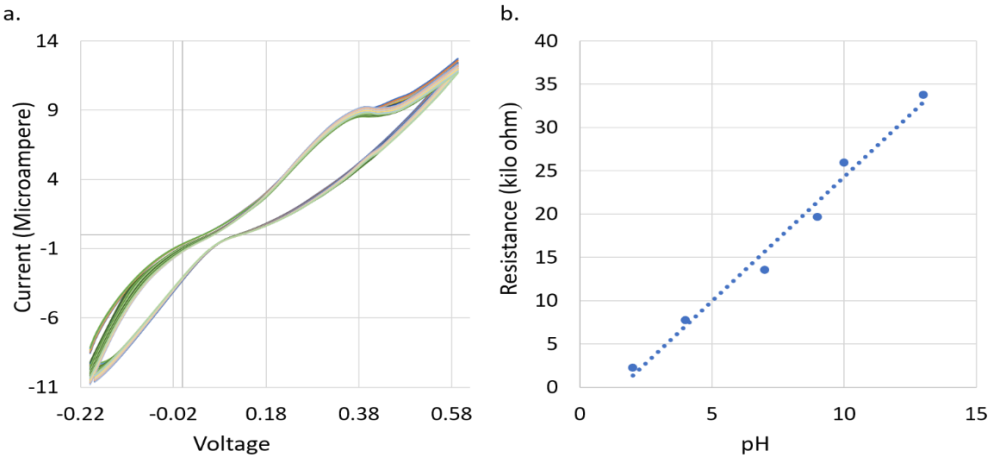

Figure 5.1. (a) Cyclic voltammetry (CV) responses for PANI deposition on the pH sensor. (b) Calibration curve of the pH sensor [76].

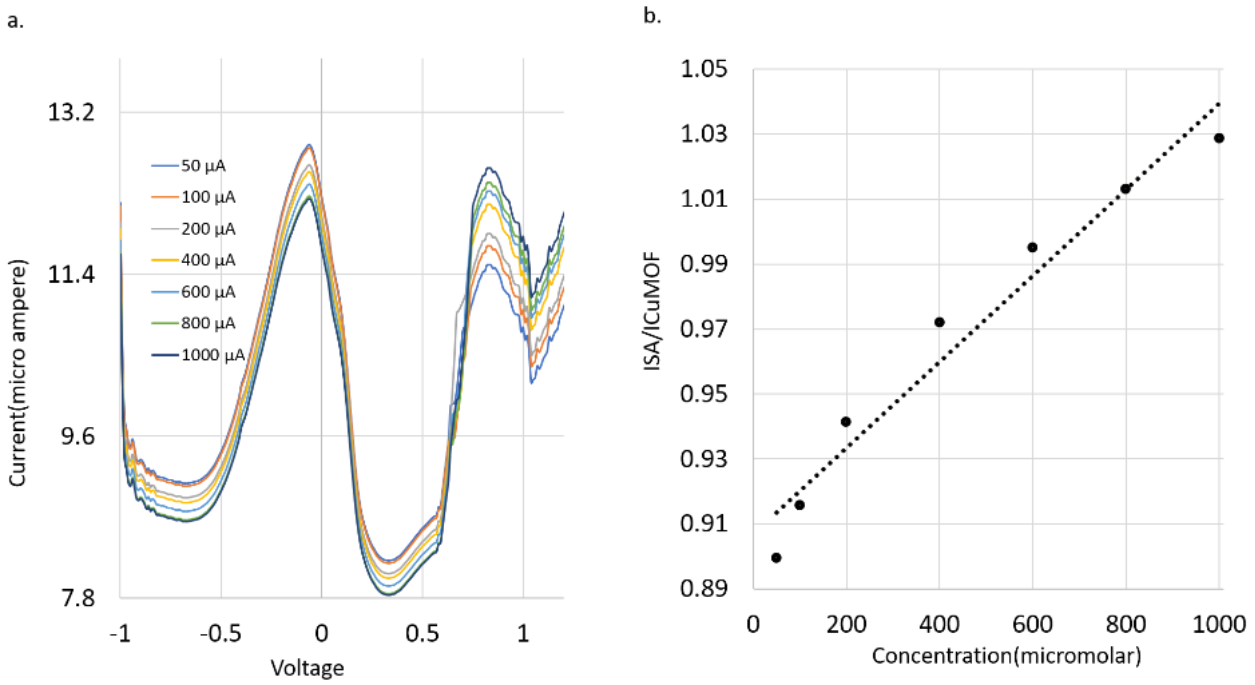

Figure 5.2. (a) Differential Pulse Voltammetry responses for different concentrations of SA. (b) Calibration curve showing I_{SA}/I_{CuMOF} vs. SA concentrations [76].

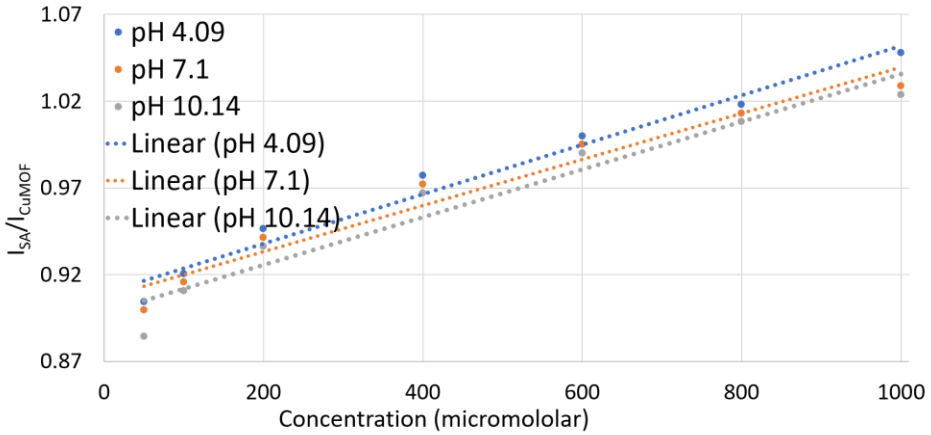

Figure 5.3. Calibration curves of the SA sensor for different pH values (4.09, 7.1, and 10.14) [76].

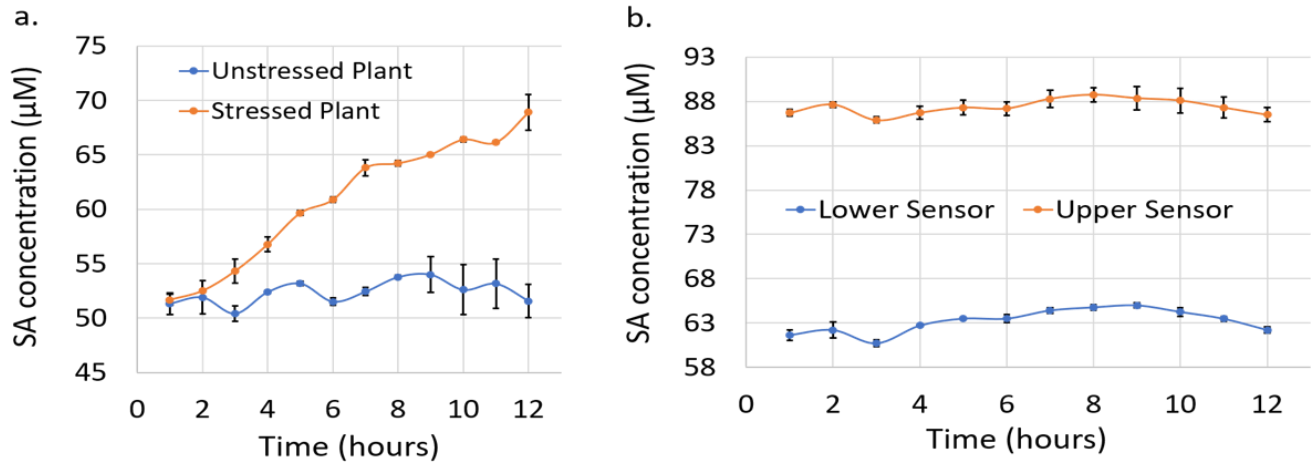

Figure 5.4. (a) SA measurement results on the stem of unstressed and water-stressed cabbage plants. (b) SA measurement results at two different locations on the same plant [76].

5.2 Microneedle based leaf sensor

The microneedle-based leaf sensor has temperature sensor incorporated with it. In this project SA is detected simultaneously with IAA.

The IAA sensor is calibrated using DPV and the calibration curve is shown in Figure 5.5. The IAA sensor is tested for selectivity, where unwanted chemical species are added including:

I) Jasmonic acid (JA)=50 µM, (II) L-Cysteine (L-Cys)=50 µM, (III) glucose=50 µM, (IV) citric acid=50 µM, (V) ascorbic acid=50 µM, (VI) a mixture of JA, L-Cys, glucose, citric acid, and ascorbic acid (50 µM each), (VII) IAA=100 µM, (VIII) a mixture of ascorbic acid, JA, L-Cys, glucose, citric acid, ascorbic acid (50 µM each), and IAA=100 µM, (IX) 200 µ), (X) a mixture of ascorbic acid, JA, L-Cys, glucose, citric acid, ascorbic acid (50 µM each), and IAA=200 µM. The IAA sensor temperature response is also checked. Both the results are delineated in Figure 5.6.

The sensor response is tested for both stressed and unstressed plants (Figure 5.7). The result is verified with HPLC. The sensor is placed in upper and lower leaves, showing the time difference between the phytohormone readings (Figure 5.8).

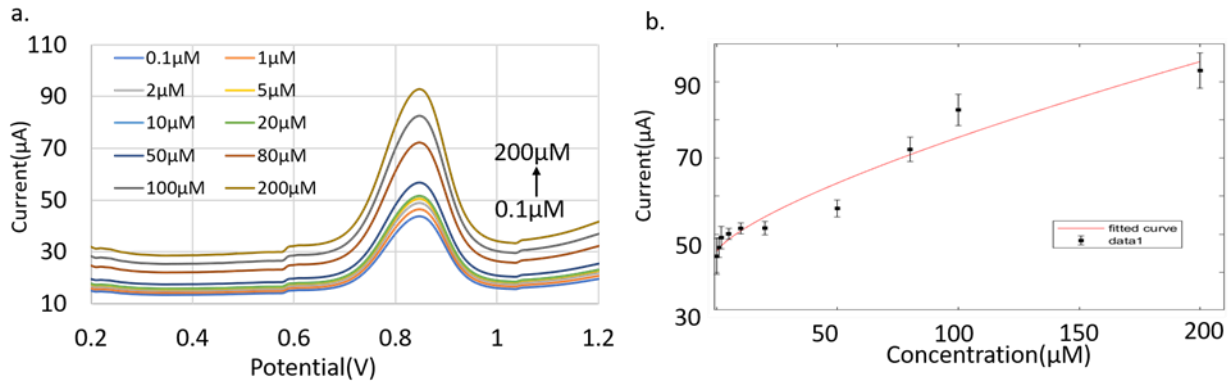

Figure 5.5. (a) The differential pulse voltammetry responses of IAA sensor for different concentrations of IAA and (b) the calibration curve of the IAA sensor [78].

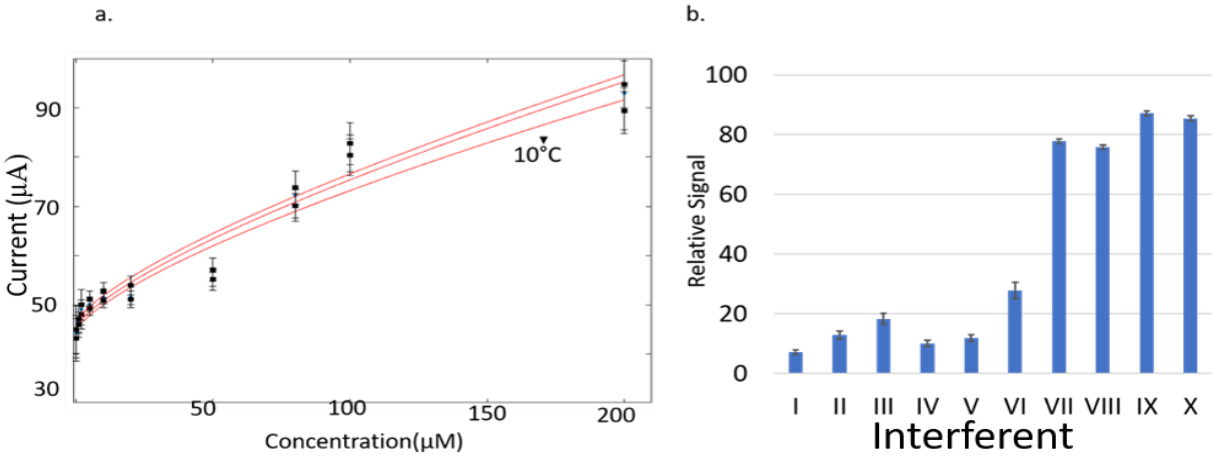

Figure 5.6: (a) Temperature response of the IAA sensor; (b) Selectivity tests of IAA sensor where i-ix means Jasmonic acid (JA)=50 µM, (II) L-Cysteine (L-Cys)=50 µM, (III) glucose=50 µM, (IV) citric acid=50 µM, (V) ascorbic acid=50 µM, (VI) a mixture of JA, L-Cys, glucose, citric acid, and ascorbic

acid (50 µM each), (VII) IAA=100 µM, (VIII) a mixture of ascorbic acid, JA, L-Cys, glucose, citric acid, ascorbic acid (50 µM each), and IAA=100 µM, (IX) 200 µ), (X) a mixture of ascorbic acid, JA, L-Cys, glucose, citric acid, ascorbic acid (50 µM each), and IAA=200 µM [78].

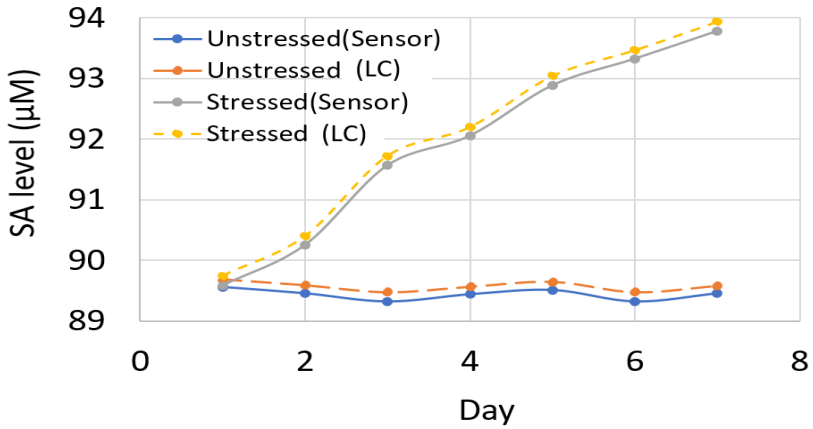

Figure 5.7. The real time SA levels on stressed and unstressed plants [78].

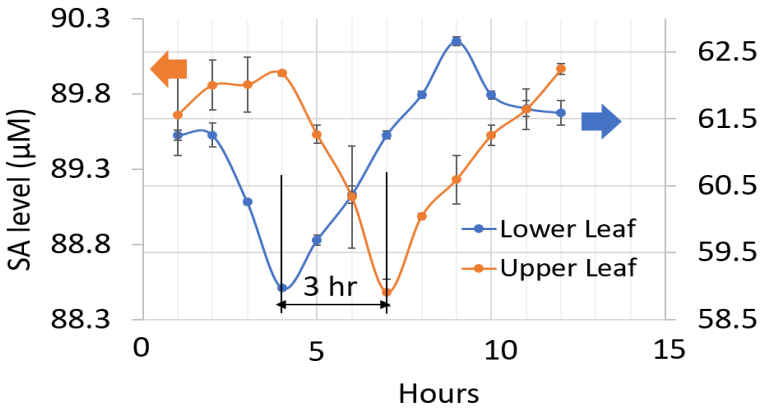

Figure 5.8. The real time SA levels on upper and lower leaves [78].

5.3 Hybrid sensor (Fruit)

The hybrid sensor suite includes SA, IAA, ethylene, and pH sensors on a single chip. The calibration curves for SA and IAA sensors at different pH levels are shown in Figure 5.9. In addition, the measurements of SA and IAA levels in a bell pepper are shown in Figure 5.10. This work has been accepted for publication at 2022 IEEE Sensors Conference [79].

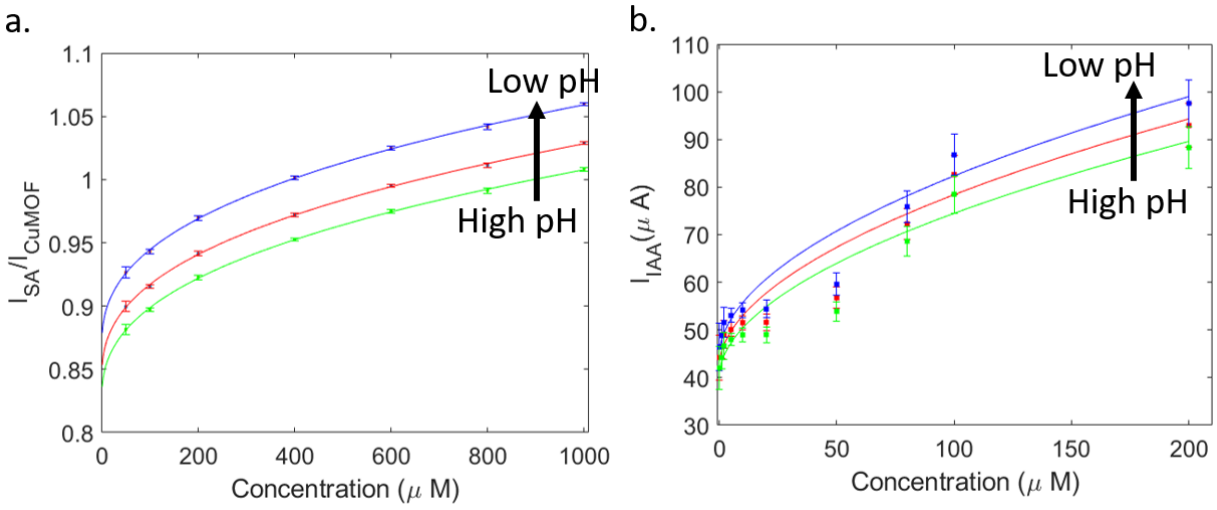

Figure 5.9: Calibration curves of (a) SA and (b) IAA sensors for different pH [79].

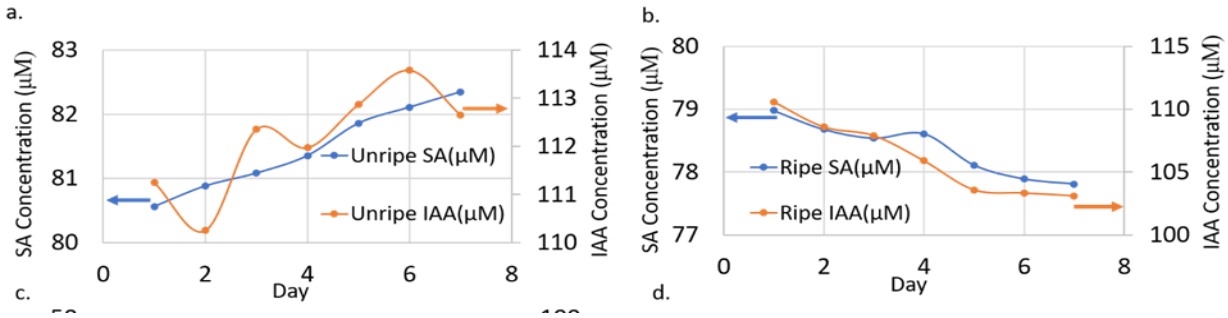

Fig. 5.10. The trend of SA and IAA in (a) unripe and (b) ripe bell peppers [79].

Chapter Six

Conclusion and Summary

In summary, in this research work wearable sensors for plants have been developed keeping in mind several research challenges such as invasive testing and response in real environment. The main contribution of this research work involves developing electrochemical sensors to detect three key phytohormones related to plant stress in a very early stage. The sensors detected salicylic acid, indole-3-acetic acid, and ethylene. This research evolves from a planar sensor that causes permanent damage to the leaf tissue to microneedle-based sensors that cause minimal damage to the leaves and fruits, while also resulting in improved sensitivity and selectivity for real-field applications. This research work involves not only laboratory experiments but also real field data collection. Another aspect of this research is that the wearable sensors have been developed for multiple parts of the plants including leaf, stem, and fruit. The leaf and stem sensor can detect the plant stress early which will help to intervene early to improve productivity while the fruit sensor indicates the ripening stage of fruits which will help harvesting at the right time.

References

[1] L. Lipper, P. Thornton, B. M. Campbell, T. Baedeker, A. Braimoh, M. Bwalya, P. Caron, A. Cattaneo, D. , Garrity, K. Henry, R. Hottle, L. Jackson, A. Jarvis, F. Kossam, W. Mann, N. McCarthy, A. Meybeck, H. Neufeldt, T. Remington, P. T. Sen, R. Sessa, R. Shula, A. Tibu, E. F. Torquebiau, *Nat. Clim. Change* 2014, *4*, 1068.

[2] R. Gebbers, V. I. Adamchuk, *Science* 2010, *327*, 828.

[3] E. Harrison, L. Monroe-Lord, A. D. Carson, A. M. Jean-Baptiste, J. Phoenix, P. Jackson, B. M. Harris, E. Asongwed, M. L. Richardson, *BMC Public Health* 2021, *21*, 755.

[4] T. Hofmann, G. V. Lowry, S. Ghoshal, N. Tufenkji, D. Brambilla, J. R. Dutcher, L. M. Gilbertson, J. P. Giraldo, J. M. Kinsella, M. P. Landry, W. Lovell, R. Naccache, M. Paret, J. A. Pedersen, J. M. Unrine, J. C. White, K. J. Wilkinson, *Nat. Food* 2020, *1*, 416.

[5] N. Suzuki, R. M. Rivero, V. Shulaev, E. Blumwald, R. Mittler, *New Phytol.* 2014, *203*, 32.

[6] H. N. Fones, D. P. Bebber, T. M. Chaloner, W. T. Kay, G. Steinberg, S. J. Gurr, *Nat. Food* 2020, *1*, 332. [7] M. C. Fisher, D. A. Henk, C. J. Briggs, J. S. Brownstein, L. C. Madoff, S. L. McCraw, S. J. Gurr, *Nature* 2012, *484*, 186.

[8] K. G. Scholthof, S. Adkins, H. Czosnek, P. Palukaitis, E. Jacquot, T. Hohn, B. Hohn, K. Saunders, T. Candresse, P. Ahlquist, C. Hemenway, G. D. Foster, *Mol. Plant Pathol.* 2011, *12*, 938.

[9] C. M. Oliveira, A. M. Auad, S. M. Mendes, M. R. Frizzas, *Crop Prot.* 2014, *56*, 50.

[10] R. J. F. Bruins, C. Shuming, C. Shijian, W. J. Mitsch, *Ecol. Eng.* 1998, *11*, 231.

[11] R. P. de S. Celedonio, L. G. Abeledo, D. J. Miralles, *Plant Soil* 2018, *429*, 469.

[12] S. Fahad, A. A. Bajwa, U. Nazir, S. A. Anjum, A. Farooq, A. Zohaib, S. Sadia, W. Nasim, S. Adkins, S. Saud, M. Z. Ihsan, H. Alharby, C. Wu, D. Wang, J. Huang, *Front. Plant Sci.* 2017, *8*, 1147.

[13] C. Guillaume, C. Isabelle, B. Marc, A. Thierry, *Plant Cell Environ.* 2018, *41*, 1008.

[14] F. M. Padilla, M. Gallardo, M. T. Pena-Fleitas, R. de Souza, R. B. Thompson, *Sensors* 2018, *18*, 2083.

[15] V. Singh, A. K. Misra, *Inf. Process. Agric.* 2017, *4*, 41.

[16] Z. Li, R. Paul, T. B. Tis, A. C. Saville, J. C. Hansel, T. Yu, J. B. Ristaino, Q. Wei, *Nat. Plants* 2019, *5*, 856.

[17] T. Liu, L. Wang, S. Zhu, C. Yang, *Agric. Sci. Technol.* 2013, *14*, 155.

[18] D. Tran, F. Dutoit, E. Najdenovska, N. Wallbridge, C. Plummer, M. Mazza, L. E. Raileanu, C. Camps, *Sci. Rep.* 2019, *9*, 17073.

[19] S. Yao, P. Ren, R. Song, Y. Liu, Q. Huang, J. Dong, B. T. O'Connor, Y. Zhu, *Adv. Mater.* 2019, *32*, 1902343.

[20] Y. Zhang, C. Chen, Y. Qiu, L. Ma, W. Qiu, R. Yu, W. Yu, X. Y. Liu, *Adv. Funct. Mater.* 2021, *31*, 2100150.

[21] A. Chhetry, S. Sharma, S. C. Barman, H. Yoon, S. Ko, C. Park, S. Yoon, H. Kim, J. Y. Park, *Adv. Funct. Mater.* 2021, *31*, 2007661.

[22] X. Peng, K. Dong, C. Ning, R. Cheng, J. Yi, Y. Zhang, F. Sheng, Z. Wu, Z. L. Wang, *Adv. Funct. Mater.* , 2021, *31*, 2103559.

[23] S. Yao, A. Myers, A. Malhotra, F. Lin, A. Bozkurt, J. F. Muth, Y. Zhu, *Adv. Healthcare Mater.* 2017, *6*, 1601159.

[24] S. Yao, P. Swetha, Y. Zhu, *Adv. Healthcare Mater.* 2017, *7*, 1700889.

[25] Y. Su, C. Chen, H. Pan, Y. Yang, G. Chen, X. Zhao, W. Li, Q. Gong, G. Xie, Y. Zhou, S. Zhang, H. Tai, Y. Jiang, J. Chen, *Adv. Funct. Mater.* 2021, *31*, 2010962.

[26] G. Lee, G. Y. Bae, J. H. Son, S. Lee, S. W. Kim, D. Kim, S. G. Lee, K. Cho, *Adv. Sci.* 2020, *7*, 2001184.

[27] J. C. Yang, J. Mun, S. Y. Kwon, S. Park, Z. Bao, S. Park, *Adv. Mater.* 2019, *31*, 1904765.

[28] X. Wang, L. Dong, H. Zhang, R. Yu, C. Pan, Z. L. Wang, *Adv. Sci.* 2015, *2*, 1500169.

[29] X. Fu, L. Wang, L. Zhao, Z. Yuan, Y. Zhang, D. Wang, D. Wang, J. Li, D. Li, V. Shulga, G. Shen, W. Han, *Adv. Funct. Mater.* 2021, *31*, 2010533.

[30] H. Yao, T. Sun, J. S. Chiam, M. Tan, K. Y. Ho, Z. Liu, B. C. K. Tee, *Adv. Funct. Mater.* 2021, *31*, 2008650.

[31] G. Lee, J. H. Son, S. Lee, S. W. Kim, D. Kim, N. N. Nguyen, S. G. Lee, K. Cho, *Adv. Sci.* 2021, *8*, 2002606.

[32] Z. Zhou, K. Chen, X. Li, S. Zhang, Y. Wu, Y. Zhou, K. Meng, C. Sun, Q. He, W. Fan, E. Fan, Z. Lin, X. Tan, W. Deng, J. Yang, J. Chen, *Nat. Electron.* 2020, *3*, 571.

[33] W. Zhou, S. Yao, H. Wang, Q. Du, Y. Ma, Y. Zhu, *ACS Nano* 2020, *14*, 5798.

[34] J. Xiong, J. Chen, P. S. Lee, *Adv. Mater.* 2020, 2002640.

[35] L. Yan, T. Zhou, L. Han, M. Zhu, Z. Cheng, D. Li, F. Ren, K. Wang, X. Lu, *Adv. Funct. Mater.* 2021, *31*, 2010465.

[36] Y. Lu, K. Xu, L. Zhang, M. Deguchi, H. Shishido, T. Arie, R. Pan, A. Hayashi, L. Shen, S. Akita, K. Takei, *ACS Nano* 2020, *14*, 10966.

[37] T. T. S. Lew, V. B. Koman, P. Gordiichuk, M. Park, M. S. Strano, *Adv. Mater. Technol.* 2019, *5*, 1900657.

[38] H. Yin, Y. Cao, B. Marelli, X. Zeng, A. J. Marson, C. Cao, *Adv. Mater.* 2021, *33*, 2007764.

[39] P. Wang, E. Lombi, F. J. Zhao, P. M. Kopittke, *Trends Plant Sci.* 2016, *21*, 699.

[40] F. Brilli, F. Loreto, I. Baccelli, *Front. Plant Sci.* 2019, *10*, 264.

[41] M. Haworth, C. Elliott-Kingston, J. C. McElwain, *J. Exp. Bot.* 2011, *62*, 2419.

[42] J. P. Giraldo, H. Wu, G. M. Newkirk, and S. Kruss. Nanobiotechnology approaches for engineering smart plant sensors. *Nature Nanotechnology*, 14: 541–553, 2019.

[43] Hayat, A., and Marty, J. L. ,2014, Sensors 14, 10432–10453.

[44] Beaver, K., Dantanarayana, A., and Minteer, S. D. ,2021, J. Phys. Chem. B 125, 11820–11834.

[45] Shi, J., Claussen, J. C., McLamore, E. S., ul Haque, A., Jaroch, D., Diggs, A. R., et al. ,2011, Nanotechnology 22, 355502.

[46] Shi, J., Zhang, H., Snyder, A., Wang, M.-, X., Xie, J., Marshall Porterfield, D., et al. ,2012Biosens. Bioelectron. 38, 314–320.

[47] Sun, L., Pan, Y., Wu, J., Zhao, D., Hui, M., Zhu, S., et al. ,2020, Sensors 20, 5512.

[48] Sun, L.-J., Feng, Q.-M., Yan, Y.-F., Pan, Z.-Q., Li, X.-H., Song, F.-M., et al., 2014, Biosensors Bioelectron. 60, 154–160.

[49] Fu, Z. Q., and Dong, X., 2013, Annu. Rev. Plant Biol. 64, 839–863.

[50] Ding, P., and Ding, Y., 2020, Trends Plant Sci. 25, 549–565.

[51] Vlot, A. C., Sales, J. H., Lenk,M., Bauer, K., Brambilla, A., Sommer, A., et al. , 2021, New Phytol. 229, 1234–1250

[52] Lee, G., Wei, Q., Zhu, Y., Emerging Wearable Sensors for Plant Health Monitoring. Adv. Funct. Mater. 2021, 31, 2106475.

[53] Gao, J., Li, H., Li, M., Wang, G., Long, Y., Li, P., et al., 2021, Anal. Chim. Acta 1145, 103–113.

[54] Teale, W. D., Paponov, I. A., and Palme, K., 2006, Nat. Rev. Mol. Cell Biol. 7, 847–859.

[55] Yang, L., Ma, Y., and Ye, J. ,2021, Biosens. Bioelectron. X 9, 100086.

[56] Li, H., Wang, C., Wang, X., Hou, P., Luo, B., Song, P., et al., 2019, Biosens. Bioelectron. 126, 193–199.

[57] Esser, B., Schnorr, J. M., and Swager, T. M., 2012, Angew. Chem. Int. Ed. 51 (23), 5752–5756.

[58] V. B. Koman, T. T. S. Lew, M. H. Wong, S. Y. Kwak, J. P. Giraldo, M. S. Strano, *Lab Chip* 2017, *17*, 4015.

[58] A. L. Fletcher, T. R. Sinclair, L. H. Allen, *Environ. Exp. Bot.* 2007, *61*, 145

[59] N. Katsoulas, A. Baille, C. Kittas, *Agric. For. Meteorol.* 2001, *106*, 233.

[60] G. W. Koch, J. S. Amthor, M. L. Goulden, *Tree Physiol.* 1994, *14*, 347

[61] Swiatek, A., Van Dongen, W., Esmans, E. L., and Van Onckelen, H., 2004, Plant Physiol. 135, 161–172.

[62] Cutler, S. R., Rodriguez, P. L., Finkelstein, R. R., and Abrams, S. R., 2010, Ann. Rev. Plant Biol. 61, 651–679.

[63] hi, G. R., Cai, Q. S., Liu, Q. Q., and Wu, L. ,2009, Acta Physiol. Plant. 31, 969–977.

[64] Lei, M., Zhu, C., Liu, Y., Karthikeyan, A. S., Bressan, R. A., Raghothama, K. G., et al.,2011, New Phytol. 189, 1084–1095

[65] Z.-H. Duan, Q.-N. Zhao, C.-Z. Li, S. Wang, Y.-D. Jiang, Y.-J. Zhang, B.-H. Liu, H.-L. Tai, *Rare Materials*, 2020,

[66] Qu, C.-C., Sun, X.-Y., Sun, W.-X., Cao, L.-X., Wang, X.-Q., He, Z.-Z., Flexible Wearables for Plants. Small 2021, 17, 2104482.

[67] M. Zhang, M. Wang, M. Zhang, L. Qiu, Y. Liu, W. Zhang, Y. Zhang, J. Hu, and G. Wu, *Nanomaterials*, 2019, *9,10*, 1399.

[68] Z. Poltarzewski, P. Staiti, V. Alderucci, W. Wieczorek, and N. Giordano, *J. Electrochem. Soc.*, 1992, 139, 3, 73-79.

[69] D. W. Dewulf and A. J. Bard, *Catalysis Letters*, 1988, 1, 73-80

[70] L. Yang, D. Chen, X. Wang, B. Luo, C. Wang, G. Gao, et al., RSC Adv, 2020, 10, pp. 38841-38846,

[71] H. J. Park, J. H. Yoon, K. G. Lee, B. G. Choi, Park et al., Nano Convergence, vol. 6, no. 9, 2019.

[72] S. Wang, W. Deng, L. Yang, Y.Tan, Q. Xie, S. Yao, ACS Appl. Mater. Interfaces, 2017, 29, 24440–24445.

[73] T. Noushin, N. I. Hossain, S Tabassum, Front. Nanotechnol., 2022, 4.

[74] S. Kundu, S. Tabassum, R. Kumar, *IEEE Sensor Journal*, 2021, 21, 17, 18837-18846

[74] N. I. Hossain and S. Tabassum, *2021 IEEE Sensors*, 2021, pp. 1-4,

[75] N. I. Hossain, T. Noushin and S. Tabassum, *2021 IEEE Sensors*, 2021, pp. 1-4

[76] N. I. Hossain and S. Tabassum, *2022, IEEE 17th International Conference on Nano/Micro Engineered and Molecular Systems (NEMS)*, 2022, pp. 312-316.

[77] Y. F. Wang, T. Sekine, Y. Takeda, J. Hong, A. Yoshida, D. Kumaki, T. Shiba, S. Tokito, *Advanced Material Technlogies*, 2021, 6, 2100731.

[78] N. I. Hossain and S. Tabassum, *2022, Hilton Head*, (Accepted for publication).

[79] N. I. Hossain and S. Tabassum, *2022 IEEE Sensors*, 2021, pp. 1-4 (Accepted for publication).

Appendix

3D – Three-dimensional printing

ABA – Abscisic acid

AuNP-GH – Gold Nanoparticle Doped Graphite Hydrogel

CA **–** Citric Acid

CB – Carbon Black

CE– Counter Electrode

CV– Cyclic Voltammetry

CuMOF – Copper Metal Organic Framework

DMF – Dimethylformamide

DPV – Differential Pulse Voltammetry

ET– Ethylene

FTIR – Fourier-Transform Infrared Spectroscopy

GA – Gibberellic Acid

HPLC – High-performance liquid chromatography

HMI – Human Machine Interface

IAA – Indole-3-Acetic Acid

I_{CuMOF} – Oxidation Current for Copper Metal Organic Framework

I_{SA} – Oxidation Current for Salicylic Acid

JA – Jasmonic Acid

LC– Liquide Chromatography

LCR– Inductance, Capacitance, and Resistance

L-Cys– L-Cysteine

LOD – Limit of Detection

NMR – Nuclear Magnetic Resonance

OA – Oleic Acid

PANI – Polyaniline

PVP– Polyvinyl pyrrolidone

RE– Reference Electrode

rGO – reduced Graphene Oxide

SA – Salicylic Acid

SEM – Scanning Electron Microscopy

SWCNT – Single Walled Carbon Nanotube

UV-Vis – Ultra Violet – Visible range

WE_{IAA} – Working electrode for Indole-3-Acetic Acid

WE_{pH} – Working electrode for pH

WE_{SA} – Working electrode for Salicylic Acid

WE_{T} – Working electrode for Temperature